

We are IntechOpen, the world's leading publisher of Open Access books Built by scientists, for scientists

5,300

Open access books available

130,000

International authors and editors

155M

Downloads

Our authors are among the

154

Countries delivered to

TOP 1%

most cited scientists

12.2%

Contributors from top 500 universities



WEB OF SCIENCE™

Selection of our books indexed in the Book Citation Index
in Web of Science™ Core Collection (BKCI)

Interested in publishing with us?
Contact book.department@intechopen.com

Numbers displayed above are based on latest data collected.

For more information visit www.intechopen.com



Chapter

The CFD Based Method for Determining Heat Transfer Correlations on Individual Rows of Plate-Fin and Tube Heat Exchangers

Dawid Taler, Jan Taler and Marcin Trojan

Abstract

The chapter provides an analytical mathematical model of a car radiator, which includes different heat transfer coefficients (HTCs) on the first and second row of pipes. The air-side HTCs in the first and second row of pipes in the first and second pass were calculated using the correlations for the Nusselt number, which were determined by CFD simulation using the ANSYS software. Mathematical models of two radiators were built, one of which was manufactured of round tubes and the other of oval tubes. The model permits the determination of thermal output of the first and second row of tubes in the first and second pass. The small relative differences between the thermal capacities of the heat exchanger occur for different and uniform HTCs. However, the heat flow rate in the first row is much greater than the heat flow in the second row if the air-side HTCs are different on the first and second tube row compared to a case where the HTC is uniform in the whole heat exchanger. The heat transfer rates in both radiators calculated using the developed mathematical model were compared with those determined experimentally. The method for modeling of plate-fin and tube heat exchanger (PFTHE) proposed in the paper does not require empirical correlations to calculate HTCs both on the air side and on the inner surfaces of pipes. The presented method of calculating PFTHEs, considering different air-side HTCs evaluated using CFD modeling, may considerably reduce the cost of experimental research concerning new design heat exchangers implemented in manufacturing.

Keywords: Air-cooled heat exchangers, Air-side Nusselt number, Different heat transfer correlation on individual pipe row, CFD modeling, Empirical heat transfer correlation

1. Introduction

Cross-flow finned heat exchangers are used in many industrial fields. In the case of heat exchangers operating at high parameters, individual round fins are welded to the outer surfaces of the tubes. On the other hand, heat exchangers in which the temperature of the working medium is just above the ambient temperature consist

of aluminum tubes fitted with aluminum fins. These are compact heat exchangers known as plate-fin and tube heat exchangers (PFTHEs).

In finned heat exchangers with both inline and staggered tube arrangements with continuous fins, the heat transfer coefficient reaches its highest values on the first tube row (laminar flow). In subsequent rows, the HTC decreases. This is due to the large HTC values in the inlet part of channels between the fins compared to the mean coefficient on the entire fin surface.

Different methods are used to calculate heat exchangers. In the ϵ -NTU (Effectiveness - Number of Transfer Units) method, one effectiveness value is determined for the entire heat exchanger [1]. In the P-NTU (Effectiveness - Number of Transfer Units) method, P efficiency is determined for each medium [2]. Both the above methods and the LMTD (Log Mean Temperature Difference) method assume a constant HTC value on the gas side.

Kuppan collected in his book [3] relations and diagrams to determine the efficiencies of typical heat exchangers. The temperature of the working media in large heat exchangers built from several rows of tubes can be determined by numerical models [4] based on the finite difference method or the finite volume method.

The determination of the average air-side HTC of PFTHEs built with one, two, three, and four rows of tubes have received much attention in the literature. For finned tube heat exchangers with more than four tube rows, the air-side average HTC for the entire heat exchanger is determined as for a heat exchanger built with four tube rows. Kim et al. in [5] proposed formulas to calculate wavy PFTHEs. The formulas are valid for both in-line and staggered tube arrangements and allow the determination of the air-side Nusselt number and the friction coefficient. On the other hand, the paper [6] describes correlations based on experimental measurements and applicable only to PFTHEs with a linear tube system. The paper [7] describes a study showing that increasing the number of tube rows in a continuous plain fin and tube heat exchanger under dehumidifying leads to a decrease in heat transfer. Similar studies were presented by Halici et al. in the paper [8].

The authors studied PFTHEs with a staggered tube arrangement, made of copper tubes and aluminum fins. The results of the study allowed the determination of friction and Colburn coefficients and HTC for air. The determined friction factor and heat transfer coefficient for wet surfaces were greater than for dry surfaces and decreased with the increasing number of pipe rows. Correlations for the Colburn factor presented in [5–8] were determined for whole finned heat exchangers. No correlations for Colburn factor were determined for individual tube rows in PFTHEs. Also in the works [9–10], the correlations determined were for the entire car radiator and not for individual rows.

Rich [11] performed a study of PFTHEs with a staggered tube arrangement with a higher number of tube rows (5 and 6 tube rows). The results also showed that the HTC on the air side decreases with the increasing number of rows. The tests were conducted for air velocity of less than 3.5 m/s and Reynolds number of 12000.

Marković et al. [12] based on experimental data proposed a formula to determine the air pressure drop in a finned heat exchanger with a staggered tube arrangement. In the paper [12], the Darcy-Weisbach friction factor on the air-side depends on the Reynolds number and the ratio of the total external surface area of the finned tube to the surface area of the unfinned tube.

The works [1, 3, 13, 14] contain information describing the effect of pipe dimensions, shape and wall thickness, fin size, the longitudinal and transverse pitch of tube spacing on heat transfer in PFTHE.

In addition, in [14], it is discussed how the heat output of the heat exchanger changes depending on different methods of heat transfer intensification on the inner surfaces of the tubes.

CFD simulations were used in [15–17] to determine the uniform heat transfer coefficient for the entire PFTHE.

Sun et al. presented the results of CFD simulations and experimental studies of the optimized PFTHE in their paper [15]. The optimization of the finned heat exchanger consisted of directing the airflow to the back of the tubes using appropriately prepared channels. This procedure was intended to stop the formation of dead zones, thus improving heat transfer and reducing the pressure drop on the air-side.

Numerical and experimental studies of different types of fins are presented in the paper [16]. Wavy and plain fins with radially spaced winglets around the tubes in the plate fin tube heat exchanger were discussed. Numerical calculations were carried out in the form of CFD simulations in which laminar flow was assumed for air velocities ranging from 1.5 m/s to 3.5 m/s. For air velocities above 3.5 m/s, the turbulent flow was assumed. On the other hand, experimental studies allowed the determination of correlations for the air-side Nusselt number.

Nagaosa in paper [17] used direct numerical simulation (DNS) to determine the air-side heat transfer correlation, which was then verified experimentally. Good agreement of the obtained results was achieved. Unfortunately, computer-based DNS calculations require a long time to perform.

When turbulent flow occurs on the air-side (high Reynolds numbers), the Nusselt number in the first pipe row of the PFTHE takes on lower values than the Nusselt numbers in the subsequent pipe rows. This phenomenon occurs both in heat exchangers made of smooth tubes [1–3] or single finned tubes [18] and in heat exchangers with continuous fins [11]. Kearney and Jacobi [18] determined by experimental study the Nusselt number for each row of tubes in cross-flow finned tube heat exchangers with two-rows of tubes. The results showed that for a heat exchanger with an in-line arrangement of tubes, the Nusselt number in the first row was 34% lower than the Nusselt number in the second row for a Reynolds number of about 5000 and 45% lower for a Reynolds number of about 28000. In a heat exchanger with a staggered arrangement of tubes, a 45% lower Nusselt number over the entire range of Reynolds numbers was obtained for the first row of tubes compared to the second row.

In the available literature, few works are describing mathematical models of heat exchangers considering different heat transfer coefficients on different rows of heat exchanger tubes. The works [19–20] used mathematical models of PFTHEs with different heat transfer coefficients on the first and second row of tubes to simulate steady-state operation. In work [21], calculations of PFTHEs operating under transient conditions were performed.

The paper [22] describes an analytical method for determining the required air mass flow rate of a heat exchanger used in the propane pre-cooling cycle of an LNG plant. The method can be used to control the air mass flow rate through the fin tubes of an air-cooled heat exchanger to control the outlet temperature of the working media.

The paper [23] deals with the numerical modeling of a heat exchanger with finned tubes with large fin pitch. Computer simulations were carried out to propose the optimal perforation size and design for maximum heat transfer coefficient. Fin-and-tube compact heat exchangers (FTCHEs) were investigated in [24]. The results of a three-dimensional CFD simulation for an FTCHE heat exchanger constructed from oval tubes with smooth and corrugated fins are shown. Thermal–hydraulic studies were carried out for Reynolds number in the range of 200–900. The computational results show that the average Nusselt number for FTCHE with corrugated fins can be increased up to 20% compared to the case with plain fins. The average performance value for the single- and three-wave finned oval tube compact heat exchangers increased by 5% and 15%, respectively, relative to the plain tube

case. CFD modeling has also been used by the authors of a paper [25] to evaluate the thermo-hydraulic conditions of heat exchangers with finned tubes of circular, oval and flat cross-sections, with in-line or staggered tube arrangements. The study was carried out for small Reynolds numbers (400–900). For the selected performance criteria, it has been shown that the oval tube with the highest axial ratio is the optimum configuration that provides a heat transfer coefficient increase of 14% at Reynolds number $Re = 400$ and 5% at Reynolds number $Re = 900$. In turn, the effect of different combinations of circular and elliptical tubes on the air-side flow and heat transfer characteristics of the heat exchanger was investigated in [26]. Inlet air velocities were in the range of 0.5–2.5 m/s. The CFD modeling results obtained show that at low inlet velocities, the system with the elliptical tube in front of the circular tube is better than the system with the circular tube alone. At higher air inlet velocities, the system composed of elliptical and circular tubes performs better than the heat exchanger with elliptical tubes alone. Also, the heat exchanger performance was found to be better when elliptical tubes were grouped in the upper region and round tubes in the lower region compared to the alternative arrangement of elliptical and round tubes.

An analytical mathematical model of a two-pass car radiator taking into account the different air-side HTC's on the first and second row of pipes was presented in this chapter. The results of modeling car radiators made of round and oval pipes were compared with the results of experimental research.

2. Mathematical model of the two-pass PFTHE with different heat transfer coefficients on each tube row

An analytical mathematical model of a two-pass radiator with two rows of pipes was developed. The first and second-row HTC's were calculated using heat transfer correlations, which were determined based on CFD (Computational Fluid Dynamics) simulations. The radiator flow diagram is shown in **Figure 1**.

The mass flow rate \dot{m}_w to the car radiator is divided into two equal parts $\dot{m}_w/2$ flowing through the first and second row of pipes in the first pass. The starting point for building a mathematical model of a car radiator is a single-pass double-row heat exchanger (first pass of two-pass heat exchanger with two rows of tubes) (**Figure 2**).

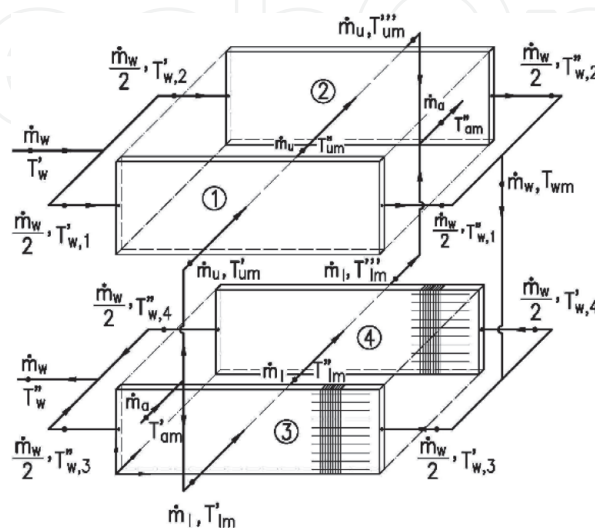


Figure 1.

Flow arrangement of the analyzed two-pass car radiator with two rows of tubes; 1 – First tube row in the first pass, 2 – second tube row in the first pass, 3 – first tube row in the second pass, 4 – second tube row in the second pass.

2.1 Analytical model for the first row of pipes

The governing energy conservation equation equations for the water and air in the first tube row are

$$\frac{dT_{w,1}(x^+)}{dx^+} = -N_w^I [T_{w,1}(x^+) - T_{ma}^I(x^+)] \quad 0 \leq x^+ \leq 1 \quad (1)$$

$$\frac{\partial T_a^I(x^+, y_1^+)}{\partial y_1^+} = N_a^I [T_{w,1}(x^+) - T_a^I(x^+, y_1^+)] \quad 0 \leq x^+ \leq 1 \quad 0 \leq y_1^+ \leq 1 \quad (2)$$

where: $x^+ = x/L_c$, $y_1^+ = y_1/p_2$ dimensionless coordinates; x, y_1 Cartesian coordinates (**Figure 2**) $T_{w,1}$ the temperature of the water in the first row of pipes, T_a^I the temperature of the air in the first row of pipes.

Two local dimensionless coordinate systems were introduced (x^+, y_1^+) and (x^+, y_2^+) (**Figure 2**). The average air temperature $T_{ma}^I(x^+)$ over the first-row width p_2 is determined by the expression

$$T_{ma}^I(x^+) = \int_{y_1^+=0}^1 T_a^I(x^+, y_1^+) dy_1^+ \quad (3)$$

The number of heat transfer units on the water-side N_w^I and air-side N_a^I are defined as follows

$$N_w^I = 2U^I A_{bout}^I / (\dot{m}_w \bar{c}_{pw}) \quad N_a^I = U^I A_{bout}^I / (\dot{m}_a \bar{c}_{pa}) \quad (4)$$

where: $A_{bout}^I = n_u^I P_{out} L_c$, n_u^I total number of pipes in the first row of the first pass, A_{bout}^I outer surface area of the bare pipes in the first row of the first pass, P_{out} outer circumference of the plain tube, L_c length of a tube in the PFTHE, The symbol \bar{c}_{pw} means the average specific heat of water in the temperature range from T_w'' to T_w' , and the average specific heat of air \bar{c}_{pa} in the temperature range from T_{am}' to T_{am}'' (**Figure 2**).

The overall HTC U^I is calculated using the expression

$$\frac{1}{U^I} = \frac{A_{bout}^I}{A_{bin}^I} \frac{1}{h_{in}^I} + \frac{A_{bout}^I}{A_{wm}^I} \frac{\delta_w}{k_w} + \frac{1}{h_{oe}^I} \quad (5)$$

where: $A_{bin}^I = n_u^I P_{in} L_c$ inner surface area of the pipes in the first row of the first pass, P_{in} inner circumference of the tube, h_{in}^I HTC on the tube inner surface in the

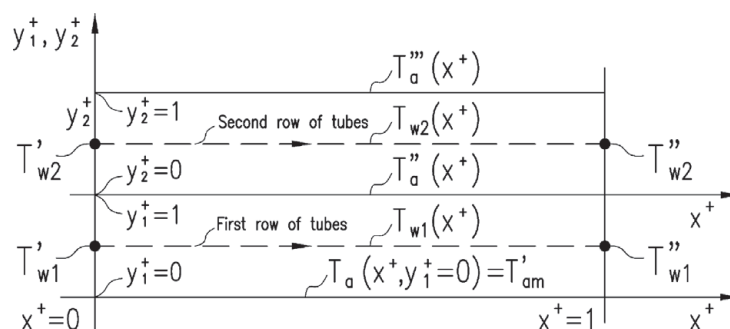


Figure 2.
 Diagram of a single-pass two-row heat exchanger.

first row of the first pass, $A_{wm} = (A_{bout}^I + A_{bin}^I)/2$ mean heat transfer area of the plain tubes in the first row of the first pass, δ_w tube wall thickness, k_w thermal conductivity of the tube material. The equivalent HTC h_{oe}^I , taking into account the heat transfer through the fins fixed to the outer surface of a plain pipe for the first row of pipes, is given by

$$h_{oe}^I = h_a^I \left[\frac{A_{bf}^I}{A_{bout}^I} + \frac{A_f^I}{A_{bout}^I} \eta_f (h_a^I) \right] \quad (6)$$

where: h_a^I air-side HTC in the first row of tubes in the first pass, A_{bf}^I tube surface area between fins, η_f fin efficiency.

The boundary conditions for Eqs. (1) and (2) are as follows

$$T_{w,1}|_{x^+=0} = T'_{w,1} \quad (7)$$

$$T_a^I|_{y_1^+=0} = T'_{am} \quad (8)$$

The solution to Eqs. (1) and (2) with boundary conditions (7) and (8) is

$$T_{w,1}(x^+) = T'_{am} + (T'_{w,1} - T'_{am}) \exp \left\{ -\frac{N_w^I}{N_a^I} [1 - \exp(-N_a^I)] x^+ \right\} \quad 0 \leq x^+ \leq 1 \quad (9)$$

$$T_a^I(x^+, y_1^+) = T_{w,1}(x^+) - [T_{w,1}(x^+) - T'_{am}] \exp(-N_a^I y_1^+) \quad 0 \leq x^+ \leq 1 \quad 0 \leq y_1^+ \leq 1 \quad (10)$$

By substituting $y_1^+ = 1$ into Eq. (10) and performing appropriate transformations the air temperature $T_a''(x^+)$ behind the first row of pipes can be obtained

$$T_a''(x^+) = T_a^I(x^+, y_1^+ = 1) = T_{w,1}(x^+) - [T_{w,1}(x^+) - T'_{am}] \exp(-N_a^I) \quad (11)$$

Expression (9) describes the temperature $T_{w,1}(x^+)$. The temperature T_{am}'' denotes the average air temperature after the first row of tubes. The temperature T_{am}'' can be calculated as follows

$$T_{am}'' = \int_0^1 T_a''(x^+) dx = T'_{am} + \frac{N_w^I}{N_a^I} (T'_{w,1} - T'_{am}) [1 - \exp(-B)] \quad (12)$$

where B stands for

$$B = \frac{N_w^I}{N_a^I} [1 - \exp(-N_a^I)] \quad (13)$$

The temperature distribution of water and air in the first row of pipes of the first pass can be determined using Eqs. (9)–(13).

2.2 Analytical model for the second row of pipes

The relevant differential equations for the second row of pipes are

$$\frac{dT_{w,2}(x^+)}{dx^+} = -N_w^{II} [T_{w,2}(x^+) - T_{ma}^{II}(x^+)] \quad 0 \leq x^+ \leq 1 \quad (14)$$

$$\frac{\partial T_a^{II}(x^+, y_2^+)}{\partial y_2^+} = N_a^{II} [T_{w,2}(x^+) - T_a^{II}(x^+, y_2^+)] \quad 0 \leq x^+ \leq 1 \quad 0 \leq y_2^+ \leq 1 \quad (15)$$

where

$$N_w^{II} = 2U^{II} A_{bout}^{II} / (\dot{m}_w \bar{c}_{pw}) \quad N_a^{II} = U^{II} A_{bout}^{II} / (\dot{m}_a \bar{c}_{pa}) \quad (16)$$

Eq. (5) allows to determine the total HTC U^{II} . Heat transfer coefficient h_{oe}^I should then be replaced by h_{oe}^{II} . The effective air-side HTC h_{oe}^{II} can be calculated using Eq. (6). HTC h_a^I should then be substituted by HTC h_a^{II} for the second row of tubes. The average air temperature over the width of the second row of pipes $T_{ma}^{II}(x^+)$ is determined as follows

$$T_{ma}^{II}(x^+) = \int_{y_2^+=0}^1 T_a^{II}(x^+, y_2^+) dy_2^+ \quad (17)$$

After taking into account that the water temperature at the inlet to the second row of pipes is $T'_{w,2}$, and the temperature of the air at the inlet to the second row of pipes is equal to the outlet temperature of the air from the first row of pipes the appropriate boundary conditions are

$$T_{w,2}|_{x^+=0} = T'_{w,2} \quad (18)$$

$$T_a^{II}|_{y_2^+=0} = T''_a(x^+) \quad (19)$$

The solution to Eqs. (14) and (15) under boundary conditions (18) and (19) is

$$T_{w,2}(x^+) = T'_{am} + \frac{E}{D-B} [\exp(-Bx^+) - \exp(-Dx^+)] + (T'_{w,2} - T'_{am}) \exp(-Dx^+) \quad (20)$$

$$0 \leq x^+ \leq 1$$

$$T_a^{II}(x^+, y_2^+) = T_{w,2}(x^+) - [T_{w,2}(x^+) - T''_a(x^+)] \exp(-N_a^{II} y_2^+) \quad (21)$$

$$0 \leq x^+ \leq 1 \quad 0 \leq y_2^+ \leq 1$$

where

$$D = \frac{N_w^{II}}{N_a^{II}} [1 - \exp(-N_a^{II})] \quad E = D (T'_{w,1} - T'_{am}) [1 - \exp(-N_a^I)] \quad (22)$$

Eq. (13) allows to calculate the coefficient B. To determine the air temperature behind the second row of pipes $T'''_a(x^+)$ (**Figure 2**), it is necessary to take into account in Eq. (21) that $y_2^+ = 1$. Then Eq. (20) should be substituted into Eq. (21). The resulting equation allows, after simple transformations, to write an expression for the air temperature $T'''_a(x^+)$ behind the second row of pipes

$$\begin{aligned}
 T_a'''(x^+) &= T_a''(x^+, y_2^+ = 1) = \\
 T_{am}' + [1 - \exp(-N_a^{II})] &\left\{ \frac{E}{D-B} [\exp(-Bx^+) - \exp(-Dx^+)] + \right. \\
 + (T_{w,2}' - T_{am}') \exp(-Dx^+) &\left. \right\} + (T_{w,1}' - T_{am}') [1 - \exp(-N_a^I)] \exp(-Bx^+ - N_a^{II}) \\
 0 \leq x^+ \leq 1 & \quad (23)
 \end{aligned}$$

The average air temperature after the second row of pipes T_{am}''' is determined by the formula

$$\begin{aligned}
 T_{am}''' &= \int_0^1 T_a'''(x^+) dx^+ = T_{am}' + [1 - \exp(-N_a^{II})] \left\{ \frac{E}{(D-B)B} [1 - \exp(-B)] - \right. \\
 - \frac{E}{(D-B)D} [1 - \exp(-D)] &+ \frac{(T_{w,2}' - T_{am}')}{D} [1 - \exp(-D)] \left. \right\} - \\
 - \frac{(T_{w,1}' - T_{am}')}{B} [1 - \exp(-N_a^I)] &[\exp(-B - N_a^{II}) - \exp(-N_a^{II})] \\
 & \quad (24)
 \end{aligned}$$

When the air-side HTC h_a^I on the first pipe row is equal to the HTC h_a^{II} on the second pipe row, then $D = B$ and the denominator $(D - B)$ is going to be zero. When $D = B$ the formula (20) requires transformation. Writing Eq. (20) as

$$\begin{aligned}
 T_{w,2}(x^+) &= T_{am}' + \frac{E \exp(-Dx^+)}{D-B} \{ \exp[(D-B)x^+] - 1 \} \\
 + (T_{w,2}' - T_{am}') \exp(-Dx^+) & \quad (25)
 \end{aligned}$$

and applying the L'Hôpital rule to an expression where, at $D = B$, the numerator and the denominator are equal to zero, one obtains

$$\begin{aligned}
 \lim_{D \rightarrow B} \frac{\exp[(D-B)x^+] - 1}{D-B} &= \lim_{z \rightarrow 0} \frac{\exp(zx^+) - 1}{z} = \lim_{z \rightarrow 0} \frac{\frac{d}{dz} [\exp(zx^+) - 1]}{\frac{dz}{dz}} = \\
 \lim_{z \rightarrow 0} \frac{x^+ \exp(zx^+)}{1} &= x^+ \\
 & \quad (26)
 \end{aligned}$$

where $z = D - B$.

Taking into account the relation (26) for $D = B$ in the formula (25), i.e. for $h_a^I = h_a^{II} = h_a$, it takes the following form

$$\begin{aligned}
 T_{w,2}(x^+) &= T_{am}' + \{ B(T_{w,1}' - T_{am}') [1 - \exp(-N_a^I)] x^+ + (T_{w,2}' - T_{am}') \} \exp(-Bx^+) \\
 0 \leq x^+ \leq 1 & \quad (27)
 \end{aligned}$$

where $N_a^I = N_a^{II} = N_a$.

If $h_a^I = h_a^{II} = h_a$, then the air temperature $T_a'''(x^+)$ after the second row of pipes is obtained with Eq. (23) after taking into account the relation (26)

$$T_a'''(x^+) = T_a''(x^+, y_2^+ = 1) = T'_{am} + [1 - \exp(-N_a^I)] \times \{ [Cx^+ + (T'_{w,1} - T'_{am})] \exp(-Bx^+) + (T'_{w,1} - T'_{am}) \exp[-(Bx^+ + N_a^I)] \} \quad 0 \leq x^+ \leq 1 \quad (28)$$

where the symbol C means

$$C = B(T'_{w,1} - T'_{am}) [1 - \exp(-N_a^I)] \quad (29)$$

3. An analytical model of a car engine radiator

The relationships derived for the single-pass double-row PFTHE, taking into account the different HTCs on the first and second row of pipes, were used to develop an analytical mathematical model of the entire radiator, the flow diagram of which is shown in **Figure 1**. This is an engine radiator with a displacement capacity of 1600 cubic centimeters.

The constructions of coolers made of round and oval tubes are described in detail in articles [9, 10], respectively. First, the temperatures $T''_{w,1}$ and $T''_{w,2}$ of the liquid at the outlet from the first pass of the cooler are calculated. Then the temperature T_{wm} of the liquid is calculated after mixing the liquid streams from the first and second pipe row (**Figure 1**). Water at the T_{wm} temperature feeds the second pass of the automobile radiator with the water mass flow rate \dot{m}_w divided into two equal parts $\dot{m}_w/2$ flowing through the first and second row of pipes. The air stream flows through the entire cross-section of the radiator. The mass flow rate through the first (upper) pass is $\dot{m}_a n_u / (n_u + n_l)$, and the second (lower) pass is $\dot{m}_a n_l / (n_u + n_l)$, respectively. The symbol \dot{m}_a denotes the mass flow rate of air flowing through the radiator. The symbols n_u and n_l stand respectively for the number of pipes in the first and second pass in the first row of tubes. The numbers n_u and n_l are equal ten and nine, respectively. Thermal calculations of the first and second row of pipes in the second (lower) pass have been carried out analogously to those of the first and second row in the first (upper) pass.

The thermal conductivity of aluminum tubes and fins was assumed to be $k_w = k_f = 207 \text{ W/(m}\cdot\text{K)}$.

4. Heat transfer correlations on the air-side

Based on CFD modeling performed in ANSY-CFX, the air-side heat transfer coefficient values were determined. The paper [19] provides a description of the method for determining the correlations for the average Nusselt number in the first and second row of pipes and for the entire cooler.

Nusselt number correlations for PFTHE from oval and round pipes are given below:

- oval pipe radiator

$$\text{Nu}_a^I = 30.7105 \text{Re}_a^{-0.24} \text{Pr}_a^{1/3} \quad 150 \leq \text{Re}_a \leq 330 \quad (30)$$

$$\text{Nu}_a^{II} = 0.0744 \text{Re}_a^{0.7069} \text{Pr}_a^{1/3} \quad 150 \leq \text{Re}_a \leq 330 \quad (31)$$

$$\text{Nu}_a = 1.0605 \text{Re}_a^{0.2974} \text{Pr}_a^{1/3} \quad 150 \leq \text{Re}_a \leq 330 \quad (32)$$

The Reynolds number on the air-side can be determined by knowing the hydraulic diameter and the air velocity in the smallest flow area. The hydraulic diameter for the oval tube cooler analyzed was $d_{h,a} = 1.42$ mm. The average Nusselt number on the first row of tubes varies very little (the exponent at the Reynolds number takes small values). Hydraulically and thermally developed laminar flow is characterized by a constant Nusselt number. Because the exponent at the Reynolds number for the second row of pipes takes larger values, the phenomenon of vortices forming near the front and rear stagnation points is more visible there. The heat transfer relation (32) for the average Nusselt number in a two-row bundle is similar to the expression for the average Nusselt number on a plane surface for thermally and hydraulically developing laminar flow, for which the exponent at the Reynolds number is $1/3$. Formulas for determining the air-side Nusselt number for an engine radiator made of circular tubes are presented below.

- round pipe radiator

$$\text{Nu}_a^I = 1.6502 \text{Re}_a^{0.2414} \text{Pr}_a^{1/3} \quad 100 \leq \text{Re}_a \leq 525 \quad (33)$$

$$\text{Nu}_a^{II} = 0.1569 \text{Re}_a^{0.5499} \text{Pr}_a^{1/3} \quad 100 \leq \text{Re}_a \leq 525 \quad (34)$$

$$\text{Nu}_a = 0.6070 \text{Re}_a^{0.3678} \text{Pr}_a^{1/3} \quad 100 \leq \text{Re}_a \leq 525 \quad (35)$$

Analyzing formulas (33) and (34), it can be observed that the exponent at Reynolds number for the first row of circular pipes is low and equals 0.2414. This indicates the dominance of laminar flow in the first row of pipes on the air-side. In the second row of tubes, the exponent at Reynolds number is higher and equals 0.5499. There are vortexes at the front and rear of the tube.

However, the average Nusselt number in the first row is higher than in the second row. This is because the inlet section is located in the gap formed by two adjacent fins, which have very high values of heat transfer coefficients at the fin surfaces. This results in a greater heat flow rate absorbed by the air in the first row than in the second row. The vortexes formed near the front and rear stagnation points on the surface of the second-row tube reduce the heat transfer to a large extent. The rotating air has a temperature close to that of the fin and pipe surfaces. From the heat transfer point of view, these are dead zones.

The comparison of the heat correlations determined by CFD modeling with the correlations determined based on experimental tests was carried out for two different car radiators. The flow arrangement of both radiators is the same (**Figure 1**). The first radiator is made of round pipes and the second one of the oval pipes.

5. Heat transfer correlations on the liquid-side

The present chapter demonstrates that by using theoretical relationships to calculate the heat transfer coefficient on the inner surfaces of the heat exchanger tubes and the use of the air-side correlations determined by CFD modeling, very similar results to experimental HTC's can be obtained.

The proposed methodology for determining the heat-transfer coefficient will reduce the cost of experimental tests for designed heat exchangers or even eliminate them. In determining the HTC for laminar flow, Gnielinski's formulas were used [27]. For the transition and turbulent flow, the formulas proposed in [28] were used.

In the range of laminar flow regime, the average HTC along the entire length of pipe L_t , assuming that the velocity profile at the pipe inlet is flat and the liquid flow is hydraulically and thermally developing, is determined by the following relationship [27].

$$\text{Nu}_{m,q} = \left[\text{Nu}_{m,q,1}^3 + 0.6^3 + (\text{Nu}_{m,q,2} - 0.6)^3 + \text{Nu}_{m,q,3}^3 \right]^{1/3} \quad \text{Re}_w \leq 2300 \quad (36)$$

The symbol $\text{Nu}_{m,q,1}$ designates the average Nusselt number for the developed laminar flow

$$\text{Nu}_{m,q,1} = \frac{48}{11} = 4.364 \quad \text{Re}_w \leq 2300 \quad (37)$$

The second Nusselt number $\text{Nu}_{m,q,2}$ represents the L ev eque solution [4] for developing flow over planar surface and $\text{Nu}_{m,q,3}$ was derived numerically for constant liquid velocity at the tube inlet

$$\text{Nu}_{m,q,2} = 3^{1/3} \Gamma(2/3) \left(\text{Re}_w \text{Pr}_w \frac{d_{hw}}{L_t} \right)^{1/3} = 1.9530 \left(\text{Re}_w \text{Pr}_w \frac{d_{hw}}{L_t} \right)^{1/3} \quad \text{Re}_w \leq 2300 \quad (38)$$

$$\text{Nu}_{m,q,3} = 0.924 \left(\text{Re}_w \frac{d_{hw}}{L_t} \right)^{1/2} \text{Pr}_w^{1/3} \quad \text{Re}_w \leq 2300 \quad (39)$$

The Nusselt number in the transition and turbulent flow range was evaluated by Taler's relationship [28].

$$\text{Nu}_w = \text{Nu}_{m,q} |_{\text{Re}_w=2300} + \frac{\frac{\xi_w}{8} (\text{Re}_w - 2300) \text{Pr}_w^{1.008}}{1.084 + 12.4 \sqrt{\frac{\xi_w}{8} (\text{Pr}_w^{2/3} - 1)}} \left[1 + \left(\frac{d_{hw}}{L_t} \right)^{2/3} \right] \quad (40)$$

$$2300 \leq \text{Re}_w \leq 10^6 \quad 0.1 \leq \text{Pr}_w \leq 1000, \quad \frac{d_{hw}}{L_t} \leq 1$$

The Darcy-Weisbach friction factor for turbulent flow, was calculated by the Taler formula [29]

$$\xi_w = (1.2776 \log \text{Re}_w - 0.406)^{-2.246} \quad 3000 \leq \text{Re}_w \quad (41)$$

The relationship for the friction factor in the transition region was obtained using the linear interpolation [29] between the value $\xi_w = 64/2300 = 0.02783$ for $\text{Re}_w = 2300$ and $\xi_w(\text{Re}_w = 3000) = 0.04355$

$$\xi_w = 0.02783 + 2.2457 \cdot 10^{-5} (\text{Re}_w - 2300) \quad 2300 \leq \text{Re}_w \leq 3000 \quad (42)$$

The Reynolds number on the water side $\text{Re}_w = w_w d_{hw} / \nu_w$ is based on the hydraulic diameter d_{hw} . The hydraulic diameter was $d_{hw} = 7.06$ mm for oval tubes and $d_{hw} = d_{in} = 6.2$ mm for circular tubes. The physical properties of the water were evaluated at the mean temperature $\bar{T}_w = (T'_w + T''_w) / 2$.

6. Experimental results

Based on the experimental testing of a car radiator made of oval and round tubes, heat transfer correlations on the air side were determined.

6.1 Engine cooler made of oval tubes

A detailed description of the test stand for experimental research of the engine radiator constructed from oval tubes can be found in [10]. The necessary parameters, including the exponent at Reynolds number, were determined from measured data. The air parameters during the radiator studies were as follows:

- Velocity: 0.98 m/s - 2.01 m/s
- Temperature: 11°C - 15°C

The water parameters at the cooler inlet were as follows:

- Volume flow rate: 627 l/h - 2421 l/h
- Temperature: 59.6°C - 72.2°C.

The Reynolds number on the air side ranged from 150 to 330, and the water-side Reynolds number in the first (upper) pass ranged from 2500 to 11,850. When determining the air-side heat transfer correlations, the water-side HTC was calculated using (36)–(42). The following Equation for the air-side Nusselt number Nu_a was found using the experimental data

$$Nu_a = x_1 Re_a^{x_2} Pr_a^{1/3} \quad 150 \leq Re_a \leq 330 \quad (43)$$

where the parameters x_1 and x_2 are

$$x_1 = 0.5162 \pm 0.0116 \quad x_2 = 0.4100 \pm 0.0041 \quad (44)$$

Numbers with a sign \pm in Eq. (44) represent half of the 95% confidence interval.

6.2 Engine cooler made of round tubes

A test stand description of a car radiator made of round tubes can be found in [10]. Flow and heat measurements allowed to determine the air-side heat transfer correlations. The air parameters during the radiator tests were as follows:

- Velocity: 0.74 m/s - 2.27 m/s
- Temperature: 3.6°C - 15.5°C

The water parameters at the cooler inlet were as follows:

- Volume flow rate: 300 l/h - 2410 l/h
- Temperature: 50.0°C - 72.0 °C.

The water flow regime changed from laminar to transitional and then to turbulent during testing. The air-side Reynolds Re_a number ranged from 150 to 560. The Reynolds number $Re_{w,u}$ on the water side in the first pass of the heat exchanger varied from 1450 to 16,100 during the test. The water-side HTC in round tubes was evaluated using the relationships (36)–(42). The following Equation for the air-side Nusselt number Nu_a was obtained using the least-squares method

$$\text{Nu}_a = x_1 \text{Re}_a^{x_2} \text{Pr}_a^{1/3} \quad 225 \leq \text{Re}_a \leq 560 \quad (45)$$

Based on the 70 data series, the following values of parameters x_1 and x_2 were found

$$x_1 = 0.5248 \pm 0.1572 \quad x_2 = 0.4189 \pm 0.0501 \quad (46)$$

Numbers with a sign \pm in Eq. (46) represent half of the 95% confidence interval.

7. Analysis and discussion of heat flow rates from water to air transferred in the entire heat exchanger and individual rows of pipes

In the case of a radiator made of oval pipes, the results of mathematical modeling and measurements are presented as a function of the Reynolds Re_a number on the air side for two selected volume flows of water $\bar{V}_w = 326.1$ liters/h and $\bar{V}_w = 1273.4$ liters/h. For a car radiator built of round tubes, the results of tests and calculations are presented as a function of the Reynolds number $\text{Re}_{w,u}$ on the water side for the first pass of the heat exchanger for the preset air velocity w_0 in front of the radiator equal to 2.27 m/s.

7.1 Engine cooler made of oval tubes

The thermal capacity of the radiator was calculated by using an analytical mathematical model of the radiator proposed in this paper, assuming the uniform air-side HTC on both rows of pipes. **Figure 3a** shows heat flow rates calculated using the mathematical model of the PFTHE for average volumetric flow rate $\bar{V}_w = 326.06$ liters/h, average air inlet temperature $\bar{T}'_{am} = 13.62^\circ\text{C}$, and average water inlet temperature $\bar{T}'_w = 59.61^\circ\text{C}$. The average values of \bar{V}_w , \bar{T}'_{am} , and \bar{T}'_w were calculated based on seven measured data sets. **Figure 3b** presents heat flow rates obtained for the following data: $\bar{V}_w = 1273.37$ liters/h, $\bar{T}'_{am} = 14.28^\circ\text{C}$ and $\bar{T}'_w = 60.51^\circ\text{C}$.

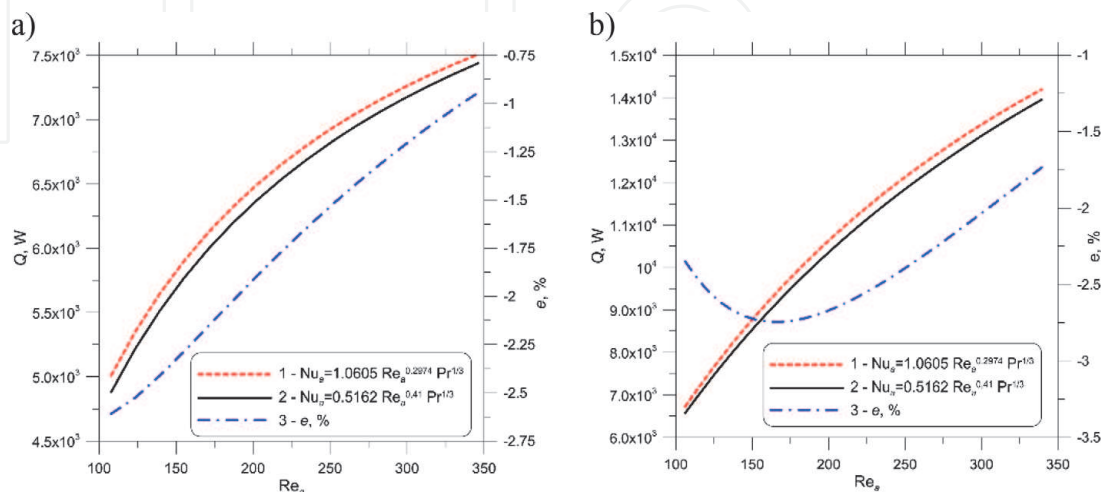


Figure 3. The heat flow rate $Q_{t,1HTC}$ from water to air in an engine cooler built with oval pipes with uniform heat transfer coefficient h_a on the air side of the whole cooler; a) $\bar{V}_w = 326.06$ liters/h, $\bar{T}'_{am} = 13.62^\circ\text{C}$ and $\bar{T}'_w = 59.61^\circ\text{C}$; b) $\bar{V}_w = 1273.37$ liters/h, $\bar{T}'_{am} = 14.28^\circ\text{C}$ and $\bar{T}'_w = 60.51^\circ\text{C}$; 1 - air-side equation for Nu_a based on the CFD modeling, 2 - air-side equation for Nu_a based on the experimental data, 3 - relative difference.

The water flow in the pipes was laminar. The Reynolds number on the water-side in the first pass was between 1222 and 1287, and in the second pass between 1358 and 1430. The velocity of the flowing air was w_0 , and its values varied from 0.71 m/s to 2.2 m/s. The heat flow rates shown in **Figure 3b** were determined for the following data: $\bar{V}_w = 1273.37$ liters/h, $\bar{T}'_{am} = 14.28^\circ\text{C}$ and $\bar{T}'_w = 60.51^\circ\text{C}$. The water flow in the pipes was turbulent. The Reynolds number in the first pass of the heat exchanger on the water-side ranged from 5238 to 5440 and in the second pass from 5820 to 5883. The air velocity before the cooler varied from 0.71 m/s to 2.2 m/s. The heat transfer coefficient on the water-side was calculated using the radiator mathematical model based on Eqs. (36)–(42). The air-side HTC was calculated using Eq. (32) based on CFD simulation (Eq. 1 in **Figure 3**) or empirical Eq. (43) (Eq. 2 in **Figure 3**).

The relative difference was calculated using the expression $e = 100(Q_2 - Q_1)/Q_2$, where Q_1 is the radiator thermal output calculated using the CFD based air-side Eq. (1) and Q_2 is the radiator thermal output calculated using the empirical Eq. (2) (**Figure 3**). The analysis of the results presented in **Figure 3a** and **b** shows that the absolute value of the difference e does not exceed 2.75%. The heat flow rates based on the measurement data $Q_{w,\text{exp}}$ and CFD simulations $Q_{w,\text{calc}}$ were calculated as follows

$$Q_{w,\text{exp}} = \dot{V}_w \rho_w (T'_{w,\text{exp}}) \bar{c}_w (T'_{w,\text{exp}} - T''_{w,\text{exp}}) \quad (47)$$

$$Q_{w,\text{calc}} = \dot{V}_w \rho_w (T'_{w,\text{exp}}) \bar{c}_w (T'_{w,\text{exp}} - T''_{w,\text{calc}}) \quad (48)$$

where: \bar{c}_w - the mean specific heat of the water in the range between the outlet $T''_{w,\text{exp}}$ (Eq. (47)) or $T''_{w,\text{calc}}$ (Eq. (48)) and inlet water temperature $T'_{w,\text{exp}}$, \dot{V}_w - water volume flow rate measured at the car radiator inlet.

The relative difference e was calculated from the following expression

$$e = \frac{Q_{w,\text{exp}} - Q_{w,\text{calc}}}{Q_{w,\text{exp}}} 100, \% \quad (49)$$

The results of measurements and calculations of the heat transfer rate Q are shown in **Figure 4**. The results are presented for seven measurement series. Calculations were performed for averaged measurement data: $\bar{V}_w = 326.06$ liters/h, $\bar{T}'_{am} = 13.62^\circ\text{C}$ and $\bar{T}'_w = 59.61^\circ\text{C}$. The mathematical model of the car radiator was used to determine the heat flow rate Q (Entries 1 and 2). The water-side heat transfer coefficient in the radiator mathematical model used was determined with Eqs. (36–42). The water flow in the cooler tubes was laminar because the water flow rate was low. The air-side HTC was determined by Eq. (32) based on CFD modeling (**Figure 4a**) or by empirical correlation (43) (**Figure 4b**). **Figure 4** also shows the relative difference values e calculated using Eq. (49). The results presented in **Figure 4a** and **b** show an excellent agreement between the calculated and measured heat flow rates when the air-side HTC is determined using Eq. (32) based on CFD modeling.

Both when using heat transfer correlation (32) based on CFD modeling and empirical correlation (43), the relative differences e range from about (–1.5%) to about 5.2%.

Figure 5 shows a similar comparison as in **Figure 4**, but for other averaged measurement data: $\bar{V}_w = 1273.37$ liters/h, $\bar{T}'_{am} = 14.28^\circ\text{C}$ and $\bar{T}'_w = 60.51^\circ\text{C}$. Due to

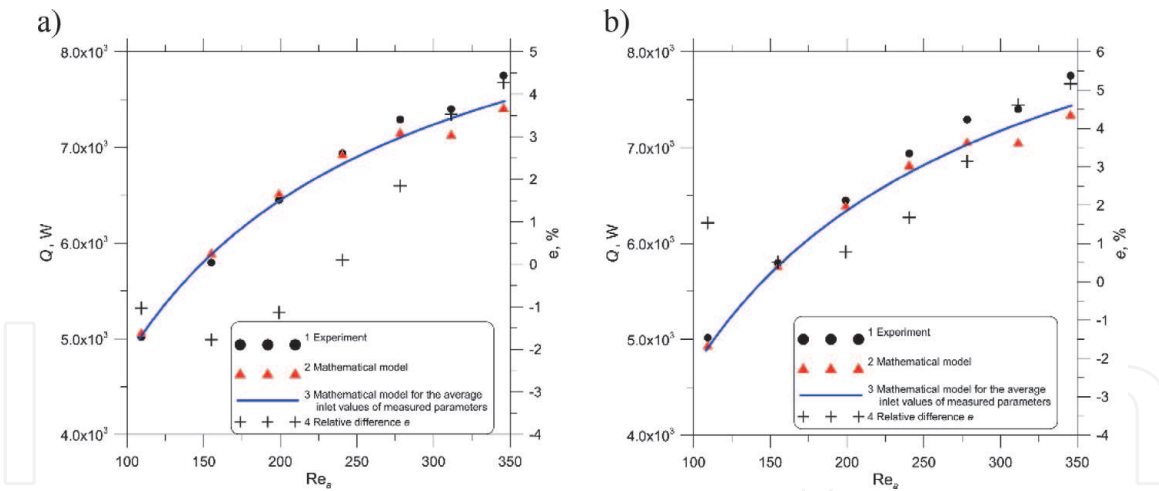


Figure 4. Heat transfer rate Q from hot water to air in a car radiator; 1 - $Q_{w,exp}$ values determined using the measurement results, 2 - heat flow rate $Q_{w,calc}$ calculated with the air-side Nusselt number Nu_a based on CFD modeling (a) or empirical correlation (b), 3 - Heat flow rate $Q_{w,calc}$ calculated with the CFD based correlation (a) or empirical correlation (b) and the average input data from 7 measurement series: $\bar{V}_w = 326.06$ liters/h, $\bar{T}_{am} = 13.62^\circ\text{C}$ and $\bar{T}_w = 59.61^\circ\text{C}$, 4 - the relative difference between $Q_{w,exp}$ and $Q_{w,calc}$ (between 1 and 2).

the higher flow rate of water flow through a car radiator equal to $\bar{V}_w = 1273.37$ liters/h, the flow regime of water in pipes was turbulent. The Reynolds number $Re_{w,u}$ on the water side of the first pass pipes was between 5238 and 5440. In the lower pass, the Reynolds number $Re_{w,l}$ was higher due to the smaller number of pipes and varied between 5820 and 5883.

It was found that the correlation for the air-side Nusselt number Nu_a determined for the entire double-row radiator based on CFD modeling provides a very good match between the calculated and measured heat flow rates transferred from hot water to air (Figures 4 and 5). Then, the heat flow rates transferred in the first and second row of pipes in both radiator passes were calculated taking into account different first and second row HTC's. The following relationships were applied to calculate heat flow rates in each row of pipes in the first and second pass

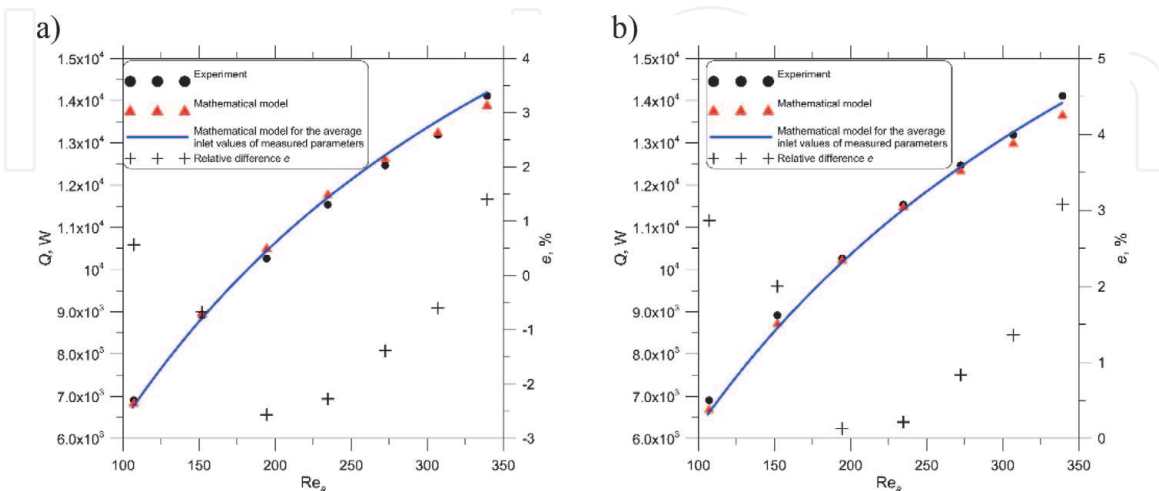


Figure 5. The heat transfer rate Q from hot water to air in a car radiator; 1 - $Q_{w,exp}$ values determined using the measurement results, 2 - heat flow rate $Q_{w,calc}$ calculated with the air-side Nusselt number Nu_a based on CFD modeling (a) or empirical correlation (b), 3 - Heat flow rate $Q_{w,calc}$ calculated with the CFD based correlation (a) or empirical correlation (b) and the average input data from 7 measurement series: $\bar{V}_w = 1273.37$ liters/h, $\bar{T}_{am} = 14.28^\circ\text{C}$ and $\bar{T}_w = 60.51^\circ\text{C}$, 4 - the relative difference between $Q_{w,exp}$ and $Q_{w,calc}$ (between 1 and 2).

Geometric data	Heat exchanger of oval pipes	Heat exchanger of round pipes
Outer tube diameter d_o , mm	Maximum tube diameter $d_{o, \max} = 11.82$ mm Minimum tube diameter $d_{o, \min} = 6.35$ mm	$d_o = 7.2$ mm
Thickness of tube wall δ_w , mm	$\delta_w = 0.4$ mm	$\delta_w = 0.5$ mm
Height p_1 and width p_2 of the apparent fin associated with one tube, mm	$p_1 = 18.5$ mm, $p_2 = 17$ mm	$p_1 = 18.5$ mm, $p_2 = 12$ mm
Fin thickness δ_f , mm	$\delta_f = 0.08$ mm	$\delta_f = 0.08$ mm
Air-side hydraulic diameter d_{ha} , mm	$d_{ha} = 1.41$ mm	$d_{ha} = 1.95$ mm
Water-side hydraulic diameter d_{hw} , mm	$d_{hw} = 7.06$ mm	$d_{hw} = d_o - 2\delta_w$ $d_{hw} = 6.2$ mm

Table 1.
Geometrical data of finned tubes in the heat exchanger made of oval and round tubes.

$$Q_{1,jHTC} = \frac{\dot{m}_w}{2} \bar{c}_w (T'_w - T''_{w,1}) \quad j = 1, 2 \quad (50)$$

$$Q_{2,jHTC} = \frac{\dot{m}_w}{2} \bar{c}_w (T'_w - T''_{w,2}) \quad j = 1, 2 \quad (51)$$

$$Q_{3,jHTC} = \frac{\dot{m}_w}{2} \bar{c}_w (T'_{wm} - T''_{w,3}) \quad j = 1, 2 \quad (52)$$

$$Q_{4,jHTC} = \frac{\dot{m}_w}{2} \bar{c}_w (T'_{wm} - T''_{w,4}) \quad j = 1, 2 \quad (53)$$

The total heat transfer rate from the air to the water was calculated using the following Equation

$$Q_{t,jHTC} = \dot{m}_w \bar{c}_w (T'_w - T''_w) \quad j = 1, 2 \quad (54)$$

The symbols $Q_{i,1HTC}$ $i = 1, \dots, 4$ designate the heat flow rate transferred in the specific pipe row (**Figure 1**) with the uniform HTC throughout the heat exchanger given by Eq. (32). The symbol $Q_{i,2HTC}$ $i = 1, \dots, 4$ stands for the heat flow rate transferred in the particular row, with the different HTCs in the first and second pipe rows. The HTC in the first row was evaluated using Eq. (30) and in the second row by applying Eq. (31). If the air-side HTC is uniform in the whole heat exchanger, then in Eqs. (50)–(54) $j = 1$ is assumed, and if the HTCs in the first and second tube row are not identical, then $j = 2$ should be taken. The relative differences e_i between the heat flow rate with different HTCs in the first and second row of tubes and the heat flow rate with uniform HTC in the entire car radiator were also calculated

$$e_i = \frac{Q_{i,2HTC} - Q_{i,1HTC}}{Q_{i,2HTC}} \cdot 100 \quad i = 1, \dots, 4 \quad (55)$$

The relative e_t difference for the whole heat exchanger was calculated with a similar formula

$$e_t = \frac{Q_{t,2HTC} - Q_{t,1HTC}}{Q_{t,2HTC}} \cdot 100 \quad (56)$$

A comparison of the first and second pipe row heat flow rates in the first and second pass of the radiator and the radiator heat output for the uniform HTC throughout the radiator and different HTCs in the first and second pipe row are shown in **Figure 6a** for $\bar{V}_w = 326.06$ liters/h and in **Figure 6b** for $\bar{V}_w = 1273.37$ liters/h.

The results presented in **Figure 6a** and **b** show that the radiator thermal output is almost identical for the uniform HTC throughout the radiator and for different HTCs in the first and second row of tubes. As shown in **Figures 5** and **6**, the radiator capacity determined by applying a mathematical model of the car cooler using the CFD based air-side correlation for the Nusselt number is very well in line with the measurements. It can also be seen that the heat flow rates exchanged in the first row of the heat exchanger, both in first and second pass, are significantly higher for different correlations for the air-side Nusselt compared to the heat flow rates obtained assuming the same HTC in both pipe rows.

The heat capacity of the heat exchanger is almost identical with the same and different HTCs on the first and second pipe row (**Figures 5** and **6**). CFD modeling and analytical formula [19] were used to determine the air temperature increase in the entire heat exchanger. A uniform HTC for the two pipe rows was then determined from the equality condition of the calculated air temperature increases. The thermal output of the entire heat exchanger will be nearly identical with uniform and different HTCs on the first and second rows of tubes. This is because the air temperature increase on both tube rows is equal to the sum of temperature increases on the first and second tube rows.

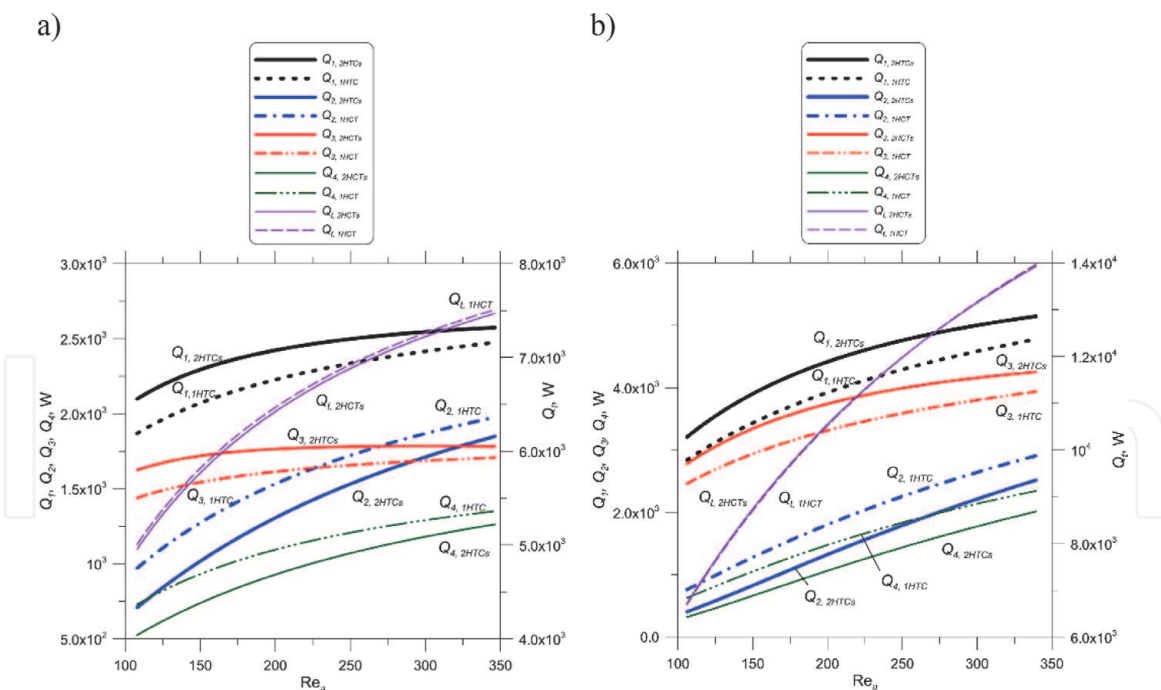


Figure 6.

Comparison of heat flow rates transferred from hot water to air in specific pipe row and entire PFTHE assuming that the air-side HTC is the same in both pipe rows with the corresponding heat transfer rates calculated using different HTCs in the first and second pipe rows; a) $\bar{V}_w = 326.06$ liters/h, $\bar{T}_{am} = 13.62^\circ\text{C}$ and $\bar{T}_w = 59.61^\circ\text{C}$, b) $\bar{V}_w = 1273.37$ liters/h, $\bar{T}_{am} = 14.28^\circ\text{C}$ and $\bar{T}_w = 60.51^\circ\text{C}$; $Q_{i,1HTC}$, $i = 1, \dots, 4$ - heat flow rates transferred in specific pipe rows (**Figure 1**) assuming the same correlation (32) for the air-side Nusselt number, $Q_{i,2HTC}$, $i = 1, \dots, 4$ - heat flow rate transferred in individual pipe rows (**Figure 1**) considering different correlations for the air-side Nusselt number, Eq. (30) for the first tube row and Eq. (31) for the second tube row, $Q_{t,1HTC}$ - car radiator output for the same heat transfer correlation (32) for all rows of pipes, $Q_{t,2HTC}$ - car radiator output for different heat transfer correlations for the first and second tube rows, Eq. (30) for the first row and Eq. (31) for the second tube row.

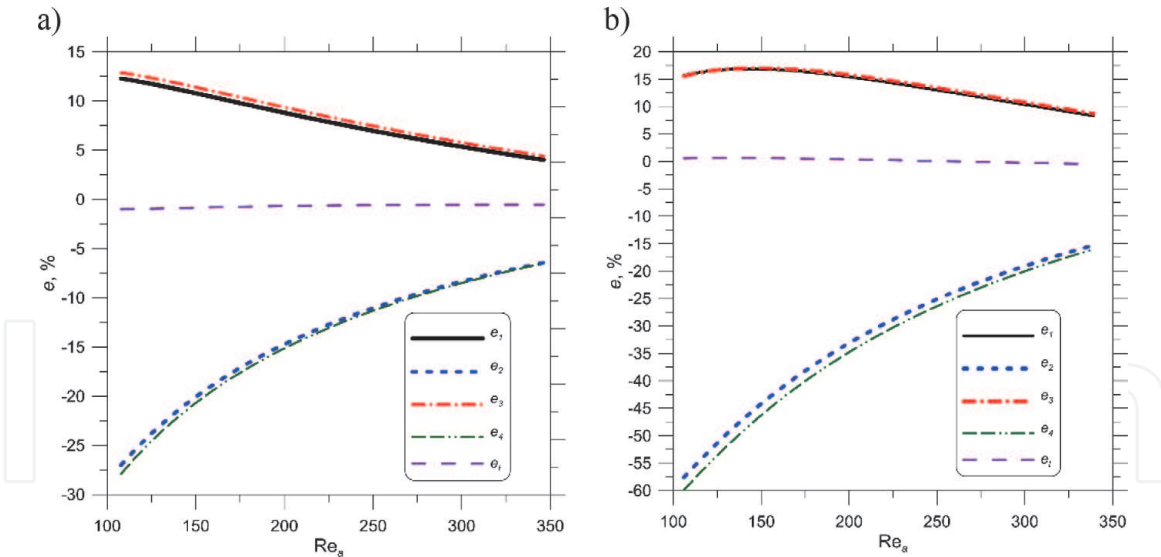


Figure 7.

The relative differences between heat flow rates for different and uniform HTCs; a) $\bar{V}_w = 326.06$ liters/h, $T'_{am} = 13.62^\circ\text{C}$ and $T'_w = 59.61^\circ\text{C}$, b) $\bar{V}_w = 1273.37$ liters/h, $T'_{am} = 14.28^\circ\text{C}$ and $T'_w = 60.51^\circ\text{C}$.

Figure 7a and **b** illustrate the higher heat absorption by the air in the first pipe row and the significant reduction of heat transfer in the second pipe row if different correlations for the Nusselt numbers in the first and second pipe row are taken into account compared to the respective outputs of the individual rows with a uniform HTC.

Figure 7a and **b** show that the more considerable differences in the exchanged heat flow through the first and second row of pipes for uniform and different HTCs are higher for the larger volume flow rate passing the cooler. The differences in the heat flow rates exchanged by the individual pipe rows with equal and different HTCs on the first and second pipe row become smaller as the air-side Reynolds number increases.

7.2 Engine cooler made of circular tubes

Figure 8 depicts a comparison of the heat flow rates for the CFD based air-side correlation (35) and empirical correlation (45) for averaged measurement

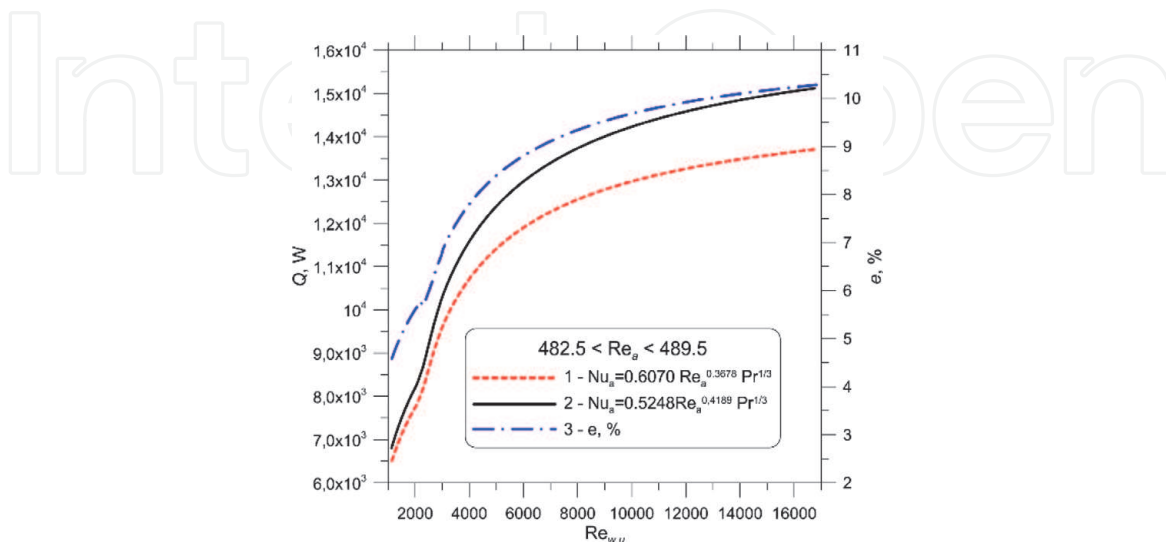


Figure 8.

The heat transfer rate $Q_{t,1HTC}$ from water to air in a car radiator made of round tubes with an equal HTC on the air side of the entire radiator as a function of the water-side Reynolds number $Re_{w,w}$; 1 - air-side correlation for Nu_a based on the CFD modeling, 2 - air-side relationship for Nu_a based on the experimental data, 3 - relative difference e .

data: $\bar{w}_0 = 2.27$ m/s, $\bar{T}'_{am} = 8.24^\circ\text{C}$ and $\bar{T}'_w = 70.56^\circ\text{C}$. The volume flow rate of water \dot{V}_w at the radiator inlet varied from 309 to 2406 liters/h. The air-side Reynolds number Re_a changed from 482.5 to 489.5 and the water-side Reynolds number $Re_{w,u}$ in the first pass of the cooler varied from 1834 to 16084.

The results presented in **Figure 8** show that the capacity of the cooler constructed with round tubes calculated for the empirical correlation to the air-side Nusselt number exceeds the capacity of the cooler calculated using the correlation to the air-side Nusselt number determined by CFD modeling. The relative difference e calculated from Eq. (49) is about 5% for a water-side Reynolds number $Re_{w,u}$ of 1800 and about 10% for a Reynolds number of 16,000 (**Figure 8**).

The relative difference e between the cooler output determined experimentally and that calculated using the mathematical model of the cooler with the air-side Nusselt number correlation obtained from CFD modeling ranges from 3% to about 8.3% (**Figure 9**). When the air-side correlation is determined experimentally, the relative difference e is smaller and ranges from -4 – 0% (**Figure 9b**).

Figure 10 shows a comparison of the heat flow rates transferred in each pipe rows assuming the same air-side heat transfer coefficient in the mathematical model of the radiator and different HTCs in the first and second tube rows.

The air in the first pipe row takes up a significantly higher heat flow rate assuming different HTCs in the first and second pipe row compared to the heat flow rate determined assuming an even HTC throughout the heat exchanger (**Figures 10 and 11**).

The relative differences e_1 and e_3 are approximately 7.5% for $Re_{w,u}$ equal to 1000 and increase with $Re_{w,u}$ to about 15% for the Reynolds number $Re_{w,u}$ equal to 18,000. The relative differences of e_2 and e_4 are approximately -8% for $Re_{w,u}$ equal to 1000 and decrease with $Re_{w,u}$ to approximately -18% for the Reynolds number $Re_{w,u}$ equal to 18,000. The results depicted in **Figures 10 and 11** show that the radiator thermal output is almost identical with an even HTC and different HTCs on both rows of pipes, despite the various capacities of the first and second rows of tubes.

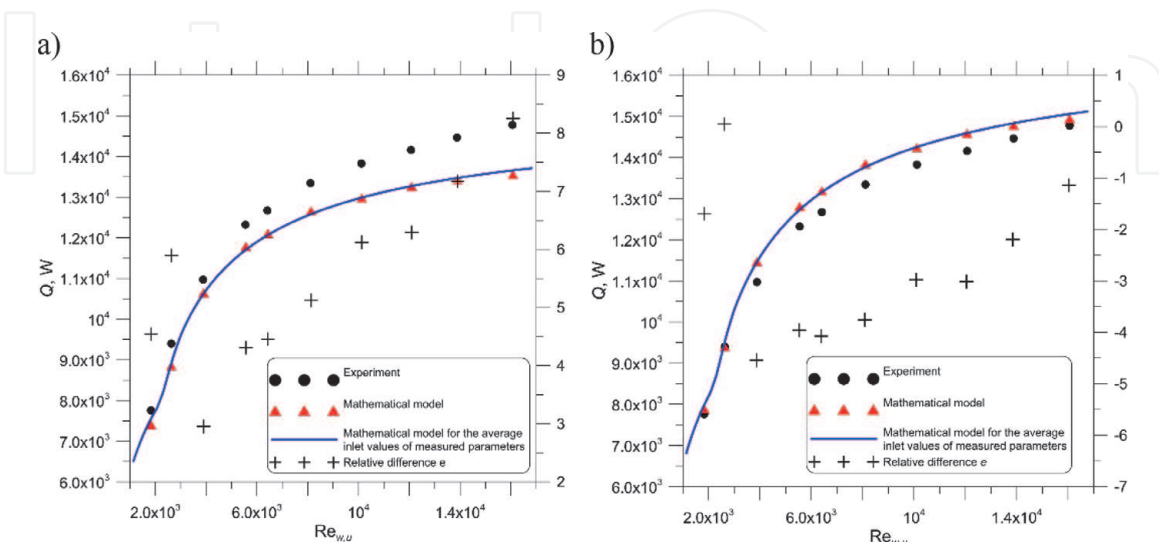


Figure 9. The comparison of heat transfer rate Q from hot water to air in a car radiator as a function of the water-side Reynolds number $Re_{w,u}$ determined experimentally and using the mathematical model of the car radiator with the uniform air-side Nusselt number Nu_a based on CFD modeling (a) and empirical correlation (b); e - relative difference.

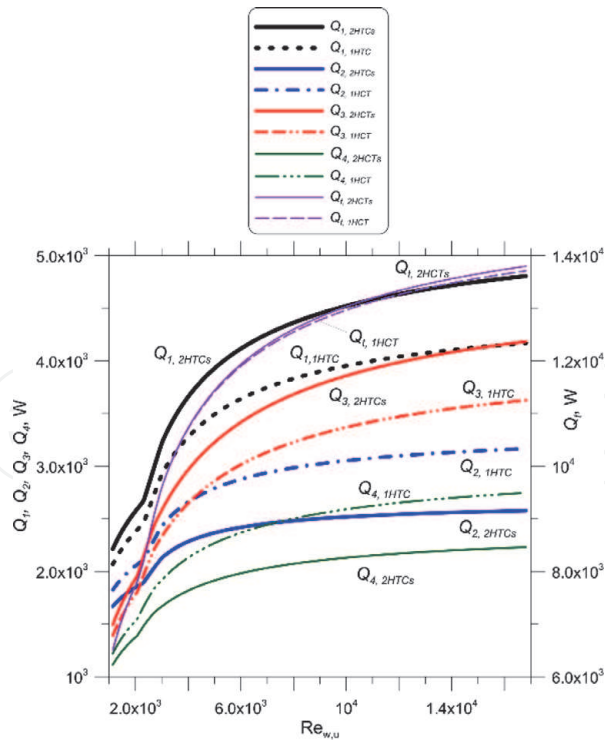


Figure 10. Heat flow rates transferred from hot water to air in specific pipe row and entire car radiator assuming that the air-side HTC is the same in both pipe rows with the corresponding heat transfer rates calculated using different HTCs in the first and second pipe rows; $\bar{w}_o = 2.27 \text{ m/s}$, $\bar{T}'_{am} = 8.24^\circ\text{C}$ and $\bar{T}'_w = 70.56^\circ\text{C}$; $Q_{i,1HTC}$, $i = 1, \dots, 4$ - heat flow rates transferred in specific pipe rows (Figure 1) assuming the same Eq. (32) for the air-side Nusselt number throughout the radiator, $Q_{i,2HTC}$, $i = 1, \dots, 4$ - heat flow rate transferred in individual pipe rows (Figure 1) assuming different equations for the air-side Nusselt number in the first and second tube row, Eq. (30) was used for the first tube row and Eq. (31) for the second tube row, $Q_{t,1HTC}$ - car radiator output for the same heat transfer Eq. (32) for all rows of pipes, $Q_{t,2HTC}$ - car radiator output for different heat transfer equations for the first and second tube rows.

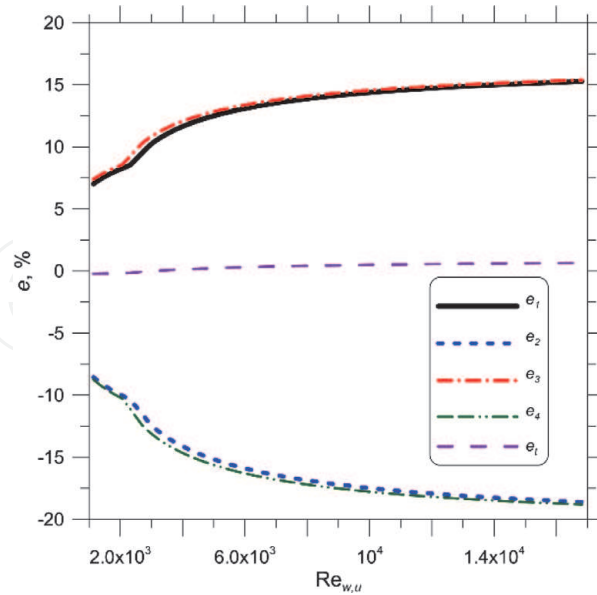


Figure 11. The relative differences e_i and e_t between heat flow rates for different and uniform HTCs calculated using Eq. (55) and (56); $\bar{w}_o = 2.27 \text{ m/s}$, $\bar{T}'_{am} = 8.24^\circ\text{C}$ and $\bar{T}'_w = 70.56^\circ\text{C}$.

8. Conclusions

An analytical model of a two-pass car radiator with two rows of pipes was built. The use of the correlations determined by CFD modeling to calculate the air-side

heat transfer coefficient was proposed. Radiators constructed from round and oval pipes were investigated. Mathematical models of car radiators were developed, in which only one average heat transfer coefficient for the entire exchanger was used, as well as different heat transfer correlations for evaluating the air-side heat transfer coefficient on the first and second row of pipes. The use of the proposed heat exchanger calculation method will allow designing a heat exchanger with the optimum number of tube rows. Taking into account different heat transfer coefficients on each row of tubes in the calculations also allows for a more accurate calculation of the thermal output of individual rows of tubes.

The water flow regime in the tubes may be laminar, transitional, or turbulent. The results of the calculations of both tested car radiators were compared with experimental data. The compatibility of calculation and measurement results is very good. The presented method of calculating plate-fin-and-tube-heat exchangers is attractive because of eliminating costly experimental research necessary for the experimental determination of the heat transfer correlations on the air and water side.

Conflict of interest

The authors declare no conflict of interest.


IntechOpen

Author details

Dawid Taler, Jan Taler* and Marcin Trojan
Department of Energy, Faculty of Environmental Engineering, Cracow University
of Technology, Cracow, Poland

*Address all correspondence to: jan.taler@pk.edu.pl

IntechOpen

© 2021 The Author(s). Licensee IntechOpen. This chapter is distributed under the terms of the Creative Commons Attribution License (<http://creativecommons.org/licenses/by/3.0>), which permits unrestricted use, distribution, and reproduction in any medium, provided the original work is properly cited. 

References

- [1] Shah RK, Sekulic DP Fundamentals of heat exchanger design. Hoboken, New Jersey, USA: Wiley 2003.
- [2] Kakaç S, Liu H, Pramuanjaroenkij A, Heat Exchangers. Selection, Rating, and Thermal Design. 3rd ed., Boca Raton, USA: CRC Press-Taylor and Francis Group 2012.
- [3] Kuppan T, Heat exchanger design handbook. 2nd ed., Boca Raton, USA: CRC Press Taylor and Francis Group 2013.
- [4] Taler D, Numerical modelling and experimental testing of heat exchangers. Berlin-Heidelberg: Springer 2019.
- [5] Kim NH, Yun JH, Webb RL, Heat transfer and friction correlations for wavy plate fin-and-tube heat exchangers. *J Heat Trans-T ASME* 1997; 119, 560–7. DOI: 10.1115/1.2824141.
- [6] Kim NH, Youn JH, Webb RL, Air-side heat transfer and friction correlations for plain fin-and-tube heat exchangers with staggered tube arrangements. *J Heat Trans-T ASME* 1999; 121, 662–7. DOI: 10.1115/1.2826030.
- [7] Wang CC, Hsieh YC, Lin YT, Performance of plate finned tube heat exchangers under dehumidifying conditions. *J Heat Trans-T ASME* 1997; 119, 109–19. DOI: 10.1115/1.2824075.
- [8] Halici F, Taymaz I, Gündüz M, The effect of the number of tube rows on heat, mass and momentum transfer in flat-plate finned tube heat exchangers. *Energy* 2001; 26, 963–972. DOI: 10.1016/S0360-5442(01)00048-2.
- [9] Taler D, Mathematical modelling and experimental study of heat transfer in a low-duty air-cooled heat exchanger. *Energy Conversion and Management* 2018; 159, 232–243. DOI: 10.1016/j.enconman.2018.01.018.
- [10] Taler D, Taler J, Prediction of heat transfer correlations in a low-loaded plate- fin-and-tube heat exchanger based on flow-thermal tests. *Applied Thermal Engineering* 2019; 148, 641–649. DOI: 10.1016/j.applthermaleng.2018.11.060.
- [11] Rich. DG, The effect of the number of tube rows on heat transfer performance of smooth plate fin-and-tube heat exchangers. *ASHRAE Tran Pt1* 1975; 81 (Paper no. 2345), 307–17. DOI: 10.1016/S0360-5442(01)00048-2.
- [12] Marković S, Jaćimović B, Genić S, Mihailović M, Milovančević U, Otović M, Air side pressure drop in plate finned tube heat exchangers. *International Journal of Refrigeration* 2019; 99, 24–29. DOI: 10.1016/j.ijrefrig.2018.11.038.
- [13] McQuiston FC, Parker J,D, Spitler JD, Heating, ventilating, and air conditioning analysis and design. 6th ed. Hoboken, New Jersey, USA: Wiley 2005.
- [14] Webb RL, Kim NH, Principles of enhanced heat transfer. 2nd. ed., Boca Raton, USA: CRC Press 2005.
- [15] Sun Ch, Lewpiriyawong N, Loong KL, Zeng S, Lee PS, Thermal enhancement of fin and tube heat exchanger with guiding channels and topology optimisation. *International Journal of Heat and Mass Transfer* 2018; 127 (Part C), 1001–1013. DOI: 10.1016/j.ijheatmasstransfer.2018.08.093.
- [16] Li MJ, Zhang H, Zhang J, Mu YT, Tian E, Dan D, Zhang XD, Tao WQ, Experimental and numerical study and comparison of performance for wavy fin and a plain fin with radiantly arranged winglets around each tube in fin-and-tube heat exchangers. *Applied Thermal*

- Engineering 2018; 133, 298–307. DOI: 10.1016/j.applthermaleng.2018.01.012.
- [17] Nagaosa RS, Turbulence model-free approach for predictions of air flow dynamics and heat transfer in a fin-and-tube exchanger. *Energy Convers Manage* 2017; 142, 414–425. DOI: 10.1016/j.enconman.2017.03.063.
- [18] Kearney SP, Jacobi AM, Local convective behaviour and fin efficiency in shallow banks of in-line and staggered, annularly finned tubes. *J Heat Trans –T ASME* 1996; 118, 317–326. DOI: 10.1115/1.2825847.
- [19] Taler D, Taler J, Trojan M, Thermal calculations of plate-fin-and-tube heat exchangers with different heat transfer coefficients on each tube row. *Energy* 2020; 203, Paper 117806, DOI: 10.1016/j.energy.2020.117806.
- [20] Taler D, Taler J, Trojan M, Experimental Verification of an Analytical Mathematical Model of a Round or Oval Tube Two-Row Car Radiator. *Energies* 2020; 13(13), 3399, DOI: <https://doi.org/10.3390/en13133399>
- [21] Taler D, Taler J, Wrona K, Transient response of a plate-fin-and-tube heat exchanger considering different heat transfer coefficients in individual tube rows. *Energy* 2020; 95 (117023), DOI: <https://doi.org/10.1016/j.energy.2020.117023>.
- [22] Fahmy MFM, Nabih HI, Impact of ambient air temperature and heat load variation on the performance of air-cooled heat exchangers in propane cycles in LNG plants - Analytical approach. *Energy Conversion and Management* 2016; 121, 22–35.
- [23] Liu X, Yu J, Yan G, A numerical study on the air-side heat transfer of perforated finned-tube heat exchangers with large fin pitches. *International Journal of Heat and Mass Transfer* 2016; 100, 199–207, DOI: 10.1016/j.ijheatmasstransfer.2016.04.081
- [24] Gholami A, Wahid MA, Mohammed HA, Thermal-hydraulic performance of fin-and-oval tube compact heat exchangers with innovative design of corrugated fin patterns. *International Journal of Heat and Mass Transfer* 2017; 106, 573–592.
- [25] Zeeshan M, Nath S, Bhanja D, Numerical study to predict optimal configuration of fin and tube compact heat exchanger with various tube shapes and spatial arrangements. *Energy Conversion and Management* 2017; 148, 737–752. DOI: 10.1016/j.enconman.2017.06.011.
- [26] Deepakkumar R, Jayavel S, Air side performance of finned-tube heat exchanger with combination of circular and elliptical tubes. *Applied Thermal Engineering* 2017; 119, 360–372.
- [27] Gnielinski V, Heat transfer in pipe flow, chapter G1. In *VDI Heat atlas*. 2nd. ed., Heidelberg: Springer 2010, 693–699. DOI: 10.1007/978-3-540-77877-6_34.
- [28] Taler D, A new heat transfer correlation for transition and turbulent fluid flow in tubes. *Int J Therm Sci* 2016; 108, 108–22. DOI: 10.1016/j.ijthermalsci.2016.04.022.
- [29] Taler D, Determining velocity and friction factor for turbulent flow in smooth tubes. *Int J Therm Sci* 2016; 105, 109–22. DOI: 10.1016/j.ijthermalsci.2016.02.011.